# Energetics of synchronized states in three-dimensional beating flagella

Clément Mettot* and Eric Lauga†

*Department of Mechanical and Aerospace Engineering, University of California San Diego, 9500 Gilman Drive, La Jolla, California 92093-0411, USA*

(Received 22 August 2011; revised manuscript received 31 October 2011; published 7 December 2011)

During collective locomotion, beating flagella of spermatozoa interact hydrodynamically and are observed experimentally to synchronize. G. I. Taylor used a small-amplitude two-dimensional sheet model to show that the rate at which swimmers do work against the fluid is minimal for in-phase beating. We use a semianalytical approach based on hydrodynamic reflections to extend these results to the small-amplitude three-dimensional beating of infinite flagellar filaments. We first consider a configuration of two parallel filaments. In the case where the beating of both flagella occurs in the same plane as that defined by their axis, in-phase beating is found to lead to an overall minimum of energy dissipation, while opposite-phase leads to a maximum. If we allow the orientation of the beating planes to vary, we find that the minimum of energy dissipation is obtained for either the in-phase or opposite-phase conformation, in a manner that depends on the flagella orientation and their relative distance. We further characterize numerically the set of optimal relative orientations. Quantitatively analogous results are obtained using a simple model based on the beating of two spheres interacting hydrodynamically in the far field. Exploiting the linearity of Stokes equation, we then extend our results to the case of three beating flagella in an aligned and triangular conformation. Consistent with Taylor's two-dimensional work, our results suggest that, from a hydrodynamic standpoint, it is more energetically favorable for spermatozoa with three-dimensional flagella to swim close to each other and with synchronized, parallel, in-phase beating.

DOI: 10.1103/PhysRevE.84.061905 PACS number(s): 87.17.Jj, 47.63.Gd

## I. INTRODUCTION

The diversity and complexity of life has long been a source of inquiry for scientists as living creatures have developed specific structural and behavioral characteristics to survive in their environment. In particular, efficient locomotion is often an important criteria for survival as it permits an organism to find food, escape predators, and reproduce. Organisms have thus evolved different modes of locomotion, many of which have been studied by the biomechanics community [1,2]. On very small scales, in particular, the study of microorganism locomotion is the object of renewed interest [3–5]. These organisms play important roles in many biological processes, including reproduction [6], bacterial infections [7], and the marine-life ecosystem [8,9]. Their study has also lead to a number of bio-inspired engineering applications, such as synthetic locomotion [10–16], mixing [17], pumping [18], transport [19], and harnessing biological organisms to perform work [20].

The physics of propulsion at a microscopic scale can be counterintuitive. The Reynolds number, which is the ratio of inertial to viscous forces on a moving organism, is typically small, so propulsion is entirely governed by viscosity [5,21]. Consequently, the equations governing the dynamics of the fluid (Stokes equations) are linear and time reversible [22]. Therefore, no locomotion is possible for a time-reversible actuation—a constraint known as the scallop theorem [21]—and as a result, computing the locomotion kinematics for a low Reynolds number swimmer can be reduced to a geometrical problem [23]. Most of the propulsion strategies employed by individual single cell or multicellular microorganisms have been extensively studied, both theoretically and experimentally, and have been reviewed in Refs. [4,5,24–30].

The individual locomotion of spermatozoa was first studied by G. I. Taylor in a landmark paper [31]. Spermatozoa propel themselves by actuating a single slender flagellum in a periodic wave-like fashion [32]. The beating is actively induced by the sliding of polymeric filaments located inside the flagellum in a structure called the axoneme, and this sliding is generated by the collective action of molecular motors [33,34]. Taylor first modeled flagella dynamics in two dimensions using a waving sheet model [31] and later extended his work to three-dimensional cylindrical flagella [35]. In both cases, he showed that the swimming velocity is nonzero at second order in the beating amplitude. Since Taylor's work, analytical and computational modeling of individual spermatozoon swimming has been the center of many studies, as reviewed in Refs. [4,5].

Beyond the locomotion of individual cells, an interesting biophysical topic is the collective dynamics of spermatozoa, which is particularly important in reproductive processes [4]. As observed experimentally, mammalian spermatozoa do not travel individually but in large populations [6]. Their collective motion presents characteristics of group dynamics, such as bundle formation and cooperation, resulting in an increased efficiency of collective swimming compared to individual cells [36–38]. The collective locomotion of other biological organisms was also extensively studied experimentally [39–42] and was the focus of several simplified modeling approaches [43–50].

At the center of the group dynamics of spermatozoa is the issue of hydrodynamic interactions between periodically beating flagella and their possible synchronization [51]. Synchronization was first modeled by Taylor who showed that, when the shapes of the flagella are prescribed to be a simple

*Current address: ONERA/DAFE, 92190 Meudon, France.
†elauga@ucsd.edu

 

traveling wave, the rate of energy dissipation between two waving sheets (equal to the rate at which the sheets are doing work) was minimum when they were beating in phase [31]. Building on numerical work using free-swimming interacting sheets [52,53], this synchronization was recently shown theoretically to arise as a geometrical symmetry-breaking mechanism [54–56]. In this paper, we propose a semianalytical method to extend Taylor's results to the small-amplitude beating of infinite three-dimensional flagella. Specifically, we characterize the dependence of the rate of energy dissipation in the fluid on the relative position, orientation, and phase of two or three nearby flagella, and we derive the configurations leading to swimming with minimum rate of working.

Our paper and our results can be summarized as follows. We first present our method and setup in Sec. II. We solve the Stokes equations using the method of reflections in cylindrical coordinates for the problem of small-amplitude beating of periodic cylindrical flagella. We thus are able to obtain the full three-dimensional flow field at leading order in the beating amplitude, as well as the rate of viscous dissipation. In Sec. III, we analyze the case of two beating flagella. After validating numerically our method, we first consider the case of beating in the plane of the two flagella, thereby directly extending Taylor's work to three dimensions. We obtain that in three dimensions, the rate of energy dissipation is still minimum for in-phase beating and maximum for out-of-phase beating. In addition, the ratio of in-plane to out-of-plane dissipation is shown to decrease when the flagella are located closer to each other. We then explore the out-of-plane beating for several orientations. We find that the minimum rate of viscous dissipation is always either the in-phase or the out-of-phase beating depending on the orientations between the two beating planes of the flagella and their relative distance. We compute the set of orientation pairs minimizing the rate of energy dissipation. In-phase planar beating is found to be the case where the rate of energy dissipation is an overall minimum. We then illustrate these results using simplified far-field hydrodynamic interactions between two periodically translating spheres, a model which displays striking similarities with our two-flagella results. In Sec. IV we exploit the linearity of Stokes equations to address the case of three flagella and present examples of the flow field and energetics for both a planar and a triangular configuration. We finish with a summary and a discussion of our results in Sec. V.

## II. SETUP AND CALCULATION METHOD

Geometrical problems such as low Reynolds number swimming are usually solved using adequate coordinate system allowing us to express easily the boundary conditions and matching them with a solution of the Stokes equations in this coordinate system. In the case of two flagella, the natural coordinate system would be the bipolar cylindrical coordinate. However, the three-dimensional Helmoltz equation for the pressure is not separable in this coordinate system [57], and to our knowledge no solution of the Stokes equations can thus be found analytically. In order to be able to compute a semianalytical solution, we thus use in this paper a reflection method [22] using cylindrical coordinates in which a general solution of the Stokes equations is known [35]. This method was previously implemented to address sedimentation [58].

We first derive below the general solution of the Stokes equation (Sec. II A) and express the no-slip boundary condition in cylindrical coordinates (Sec. II B). We then detail how the reflection method is implemented (Sec. II C), and explain how we obtain our solution by solving a linear system (Sec. II D). We finally derive the formula for the rate of viscous dissipation during the motion of the flagella (Sec. II E).

### A. General solution of the Stokes equations

Our setup is illustrated in Fig. 1. We model the flagella as identical infinite cylinders of radius $R$ separated by a distance $a$ and immersed in a fluid of shear viscosity $\mu$. The periodic beating of the flagella is assumed to be described by a sinusoidal wave of vertical displacement of amplitude $b$, wave number $k$, phase velocity $U$, and phase $\phi_i$ propagating toward the $-z$ direction. The wave motion of each flagellum is assumed to occur in a plane that makes an angle $\beta_i$ with the $(x,z)$ plane. Without loss of generality, we can choose the phases of the two flagella to be $\phi_2 = -\phi_1 = -\phi$, so that the phase difference $\Delta\phi = \phi_2 - \phi_1 = 2\phi$ is characterized by a single parameter $\phi \in [0,\pi/2]$ (if the phases are not equal and opposite, they can be made to be by a simple shift of the

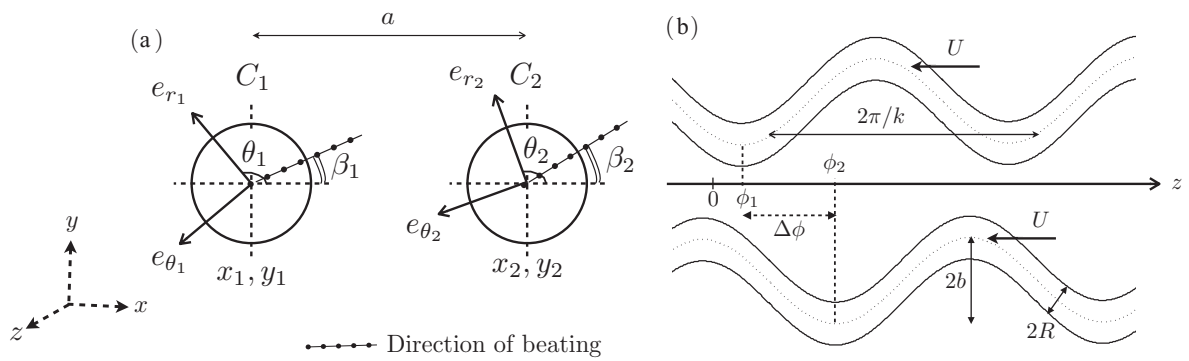


FIG. 1. Modeling the beating of two nearby flagella by two infinite cylinders deformed by a planar wave of the form $b\sin(kz + kUt + \phi_i)$ propagating in the $-z$ direction and at an angle $\beta_i$ with respect to the $(x,z)$ plane (see text for notation). (a) Cross section of the two cylindrical flagella in the $(x,y)$ plane. (b) Cross section of the $(x,z)$ plane for the special case $\beta_1 = \beta_2 = 0$.

origin of the coordinate system). We designate the two flagellar filaments by $C_1$ and $C_2$ and use the $C_1$ and $C_2$ cylindrical coordinate systems from the center of each cylinder. We aim at deriving the flow field asymptotically for small amplitude deformation $kb \ll 1$.

For the sake of simplicity, we will work using the following natural dimensionless variables

$$r^* = kr, \quad z^* = kz, \quad \mathbf{u}^* = \frac{\mathbf{u}}{Ukb}, \tag{1}$$

$$p^* = \frac{p}{\mu bk^2 U}, \quad \boldsymbol{\sigma}^* = \frac{\boldsymbol{\sigma}}{\mu bk^2 U}, \quad W^* = \frac{W}{\mu Rb^2 k^3 U^2}, \tag{2}$$

where $\mathbf{u}$ designates the fluid velocity, $p$ its pressure, $\boldsymbol{\sigma}$ the stress tensor in the fluid, and $W$ the rate of energy dissipation. As the amplitude of the beating $b$ only appears as a factor in our variables, we impose it to be $b = 1$, choosing then adequate values of $k$ such that $kb \ll 1$. Omitting in the rest of the paper the $^*$ symbols for the sake of simplicity, the dimensionless Stokes equations are given by

$$\boldsymbol{\nabla} p = \nabla^2 \mathbf{u}, \quad \nabla \cdot \mathbf{u} = 0. \tag{3}$$

Taking the divergence of Eq. (3) leads to $\nabla^2 p = 0$. A solution of the harmonic equation for the pressure is, at the first order in $kb$, $p = p_1(r,\theta)(A\cos s + B\sin s)$ with $s = z + kUt$, so that

$$\left(\frac{\partial^2}{\partial r^2} + \frac{1}{r}\frac{\partial}{\partial r} + \frac{1}{r^2}\frac{\partial^2}{\partial \theta^2} - 1\right) p_1 = 0. \tag{4}$$

Separating $p_1 = f(r)g(\theta)$, we get

$$\frac{r^2}{f}\frac{\partial^2 f}{\partial r^2} + \frac{r}{f}\frac{\partial f}{\partial r} - r^2 = -\frac{1}{g}\frac{\partial^2 g}{\partial \theta^2} = n^2. \tag{5}$$

Solutions that are decreasing at infinity are [59]

$$f(r) = f_1 K_n(r), \tag{6}$$

$$g(\theta) = g_1 \cos n\theta + g_2 \sin n\theta, \tag{7}$$

where $K_n$ are the modified Bessel functions of the second kind of order $n$, and $f_1, g_1, g_2$ are constants. The general form of the pressure can therefore be expressed as

$$p = \sum_n (A_n \cos n\theta + B_n \sin n\theta) K_n(r)\cos(s) + (a_n \cos n\theta + b_n \sin n\theta) K_n(r)\sin(s). \tag{8}$$

We will here solve the velocity equations associated with the $\cos s$ part of the pressure, as the resolution for the $\sin s$ part is similar. The momentum and continuity equations in cylindrical coordinates are given by

$$\frac{\partial p}{\partial r} = \nabla^2 u - \frac{u}{r^2} - \frac{2}{r^2}\frac{\partial v}{\partial \theta}, \tag{9}$$

$$\frac{1}{r}\frac{\partial p}{\partial \theta} = \nabla^2 v - \frac{v}{r^2} + \frac{2}{r^2}\frac{\partial u}{\partial \theta}, \tag{10}$$

$$\frac{\partial p}{\partial z} = \nabla^2 w, \tag{11}$$

$$\frac{\partial u}{\partial r} + \frac{u}{r} + \frac{1}{r}\frac{\partial v}{\partial \theta} + \frac{\partial w}{\partial z} = 0. \tag{12}$$

By the form of Eq. (8), we expect the velocity components to be of the form

$$u = \sum_n \left(u_1^n \cos n\theta + u_2^n \sin n\theta\right)\cos s, \tag{13}$$

$$v = \sum_n \left(v_1^n \cos n\theta + v_2^n \sin n\theta\right)\cos s, \tag{14}$$

$$w = \sum_n \left(w_1^n \cos n\theta + w_2^n \sin n\theta\right)\sin s, \tag{15}$$

where $u_i^n, v_i^n, w_i^n$ are functions of $r$ only. Inserting Eqs. (13)–(15) into equations Eq. (9) and (10), separating the terms in $\cos\theta$ and $\sin\theta$, then adding and subtracting them we get for $u_1^n$ and $v_2^n$

$$\left[\frac{\partial^2}{\partial r^2} + \frac{1}{r}\frac{\partial}{\partial r} - \left(1 + \frac{(n+1)^2}{r^2}\right)\right]\left(u_1^n + v_2^n\right) = A_n\left(K_n' - \frac{n}{r}K_n\right), \tag{16}$$

$$\left[\frac{\partial^2}{\partial r^2} + \frac{1}{r}\frac{\partial}{\partial r} - \left(1 + \frac{(n-1)^2}{r^2}\right)\right]\left(u_1^n - v_2^n\right) = A_n\left(K_n' + \frac{n}{r}K_n\right), \tag{17}$$

Equations (16) and (17) were solved by Taylor in his paper on single three-dimensional flagellum [35]. We get equivalent equations on $u_2^n$ and $-v_1^n$ so that $u_2^n$ and $v_1^n$ follow the same dependence on $r$ as, respectively, $u_1^n$ and $v_2^n$ with different constants. Using Taylor's work we thus get

$$2u_1^n = C_n K_{n+1}(r) + D_n K_{n-1}(r) + A_n r K_n(r), \tag{18}$$

$$2v_2^n = C_n K_{n+1}(r) - D_n K_{n-1}(r), \tag{19}$$

$$2u_2^n = E_n K_{n+1}(r) + F_n K_{n-1}(r) + B_n r K_n(r), \tag{20}$$

$$2v_1^n = F_n K_{n-1}(r) - E_n K_{n+1}(r). \tag{21}$$

The $w$ component can be computed from $u$ and $v$ using the continuity equation, Eq. (12), leading to

$$-w_1^n = \frac{\partial u_1^n}{\partial r} + \frac{u_1^n + n v_2^n}{r}, \quad -w_2^n = \frac{\partial u_2^n}{\partial r} + \frac{u_2^n - n v_1^n}{r}. \tag{22}$$

Using recurrence formulas for Bessel functions [59], we finally obtain

$$2w_1^n = (C_n + D_n) K_n + A_n (r K_{n-1} + (n-2)K_n), \tag{23}$$

$$2w_2^n = (E_n + F_n) K_n + B_n (r K_{n-1} + (n-2)K_n). \tag{24}$$

The complete solution of the Stokes equations in cylindrical coordinates to the first order in $kb$ is therefore finally given by

$$2u = \sum_n \left(U_1^n(r)\cos n\theta + U_2^n(r)\sin n\theta\right)\cos s + \left(u_1^n(r)\cos n\theta + u_2^n(r)\sin n\theta\right)\sin s, \tag{25}$$

$$2v = \sum_n \left(V_1^n(r)\cos n\theta + V_2^n(r)\sin n\theta\right)\cos s + \left(v_1^n(r)\cos n\theta + v_2^n(r)\sin n\theta\right)\sin s, \tag{26}$$

$$2w = \sum_n \left(w_1^n(r)\cos n\theta + w_2^n(r)\sin n\theta\right)\cos s + \left(W_1^n(r)\cos n\theta + W_2^n(r)\sin n\theta\right)\sin s, \tag{27}$$

with

$$U_1^n(r) = C_n K_{n+1} + D_n K_{n-1} + A_n r K_n, \quad (28)$$
$$U_2^n(r) = E_n K_{n+1} + F_n K_{n-1} + B_n r K_n, \quad (29)$$
$$V_1^n(r) = F_n K_{n-1} - E_n K_{n+1}, \quad (30)$$
$$V_2^n(r) = C_n K_{n+1} - D_n K_{n-1}, \quad (31)$$
$$W_1^n(r) = (C_n + D_n) K_n + A_n [r K_{n-1} + (n-2) K_n], \quad (32)$$
$$W_2^n(r) = (E_n + F_n) K_n + B_n [r K_{n-1} + (n-2) K_n]. \quad (33)$$

From the symmetry of the equations it is not surprising that the $f_k^n$ functions have the same dependence on $r$ as the corresponding $F_k^n$ functions but with different constants.

### B. Boundary conditions

We will voluntarily keep the notation general in this subsection as the boundary conditions are the same on both flagella provided that we use the adequate index. Since we are interested in the leading-order flow problem, the surface of the cylindrical filament is characterized by the dimensionless shape $r = kR$ for all $z$, with O($kb$) flow boundary conditions arising from the flagellum motion. We assume that the cross sections of the cylinders remain circular while moving as rigid laminae parallel to the plane $(x, y)$. Given the notation used for the flagella beating plane as shown in Fig. 1, the velocity of each point at the surface of the cylindrical filament can be written, noting $(x_i, y_i)$ their instantaneous dimensional position, as

$$x_i = x_0 + b \cos\beta \sin(s + \phi), \quad (34)$$
$$y_i = y_0 + b \sin\beta \sin(s + \phi). \quad (35)$$

The O($bk$) dimensionless velocity at the surface of the flagellum is therefore given by

$$\mathbf{u} = \frac{\partial x_i}{\partial t}\mathbf{e_x} + \frac{\partial y_i}{\partial t}\mathbf{e_y}, \quad (36)$$
$$= [\cos\beta \cos(s + \phi)\,\mathbf{e_x} + \sin\beta \cos(s + \phi)\,\mathbf{e_y}]. \quad (37)$$

The no-slip condition imposes the fluid velocity $\mathbf{u}$ to be equal to the velocity of the flagellum on its surface, so that to first order in the beating amplitude the boundary conditions are given by

$$u_r\,|_{r=kR} = \cos(s + \phi)[\cos\beta \cos\theta + \sin\beta \sin\theta], \quad (38)$$
$$u_\theta\,|_{r=kR} = \cos(s + \phi)[\sin\beta \cos\theta - \cos\beta \sin\theta], \quad (39)$$
$$u_z\,|_{r=kR} = 0. \quad (40)$$

[Note that Eq. (40) is a consequence of the fact that by symmetry no swimming is expected at leading order]. These relations can be expressed in terms of the first mode of the general solution, Eqs. (25)–(27), with

$$2U_1^1 = \cos\phi \cos\beta, \quad 2V_2^1 = -\cos\phi \cos\beta, \quad (41)$$
$$2U_2^1 = \cos\phi \sin\beta, \quad 2V_1^1 = \cos\phi \sin\beta, \quad (42)$$

and the $w$ components being equal to zero. With $r = kR$ and $K_n \equiv K_n(r)$ and defining

$$\Phi(r) \equiv r K_1 \left( \frac{1}{2} + \frac{1}{2}\frac{K_0}{K_2} - \left[\frac{K_0}{K_1}\right]^2 \right) + K_0 \quad (43)$$

and

$$f_a \equiv \frac{2}{\Phi(r)}, \quad f_c \equiv \frac{r K_1}{K_2 \Phi(r)}, \quad f_d \equiv \frac{2}{K_0}\left(1 - \frac{1}{2}\frac{r K_1}{\Phi(r)}\right), \quad (44)$$

the linear system, Eqs. (41) and (42), can be inverted using Taylor's results [35], leading to the set of coefficients given by

$$A_1 = f_a \cos\phi \cos\beta, \quad C_1 = f_c \cos\phi \cos\beta, \quad (45)$$
$$D_1 = f_d \cos\phi \cos\beta, \quad B_1 = f_a \cos\phi \sin\beta, \quad (46)$$
$$E_1 = f_c \cos\phi \sin\beta, \quad F_1 = f_d \cos\phi \sin\beta. \quad (47)$$

Using this set of coefficients we will designate by $\mathbf{U_1}$ and $\mathbf{U_2}$ the velocity fields defined, respectively, on the flagella $C_1$ and $C_2$. They correspond to the velocity fields induced by each individual flagellum so that $\mathbf{U_1}$ verifies the appropriate boundary condition on $C_1$, and $\mathbf{U_2}$ verifies the one on $C_2$.

### C. Reflection method

We detail here the basic principles of the reflection method as presented in Ref. [22]. The linearity of the Stokes equations allows us to decompose our solution $\{\mathbf{u}, p\}$ as the linear superposition of two flows: one due to the motion of $C_1$ and another due to the motion of $C_2$, respectively indexed 1 and 2, each one being a solution of the Stokes equations and vanishing at infinity, i.e.,

$$\mathbf{u} = \mathbf{u_1} + \mathbf{u_2}, \quad p = p_1 + p_2, \quad (48)$$
$$\mathbf{u}\,|_{C_1} = \mathbf{U_1}, \quad \mathbf{u}\,|_{C_2} = \mathbf{U_2}. \quad (49)$$

In order for $\mathbf{u}$ to be the solution of our problem, $\mathbf{u_1}$ and $\mathbf{u_2}$ must verify the boundary conditions

$$\mathbf{u_1}_{|C1} = \mathbf{U_1}, \quad \mathbf{u_1}_{|C2} = 0, \quad (50)$$
$$\mathbf{u_2}_{|C2} = \mathbf{U_2}, \quad \mathbf{u_2}_{|C1} = 0. \quad (51)$$

We detail below the procedure to compute $\mathbf{u_1}$, which, by symmetry, is the same as the one used to compute $\mathbf{u_2}$. We decompose $\mathbf{u_1}$ as a sum of reflections, each one being a solution of the Stokes equations and vanishing at infinity:

$$\mathbf{u_1} = \sum_{i=0}^{\infty} \mathbf{u}^{1,i}. \quad (52)$$

The sum of the reflections must verify the boundary conditions

$$\sum_{i=0}^{\infty} \mathbf{u}^{1,i}_{|C1} = \mathbf{U_1}, \quad \sum_{i=0}^{\infty} \mathbf{u}^{1,i}_{|C2} = \mathbf{0}. \quad (53)$$

The previous relations are verified, provided that

$$\mathbf{u}^{1,0}_{|C1} = \mathbf{U_1}, \quad \mathbf{u}^{1,2i}_{|C1} = -\mathbf{u}^{1,2i-1}_{|C1}, \quad \mathbf{u}^{1,2i+1}_{|C2} = -\mathbf{u}^{1,2i}_{|C2}, \quad (54)$$

where the velocities $\mathbf{u}^{1,2i}$ are solutions defined from $C_1$ in $C_1$ coordinates, while the velocities $\mathbf{u}^{1,2i+1}$are defined from $C_2$ in $C_2$ coordinates, so that each new reflection is defined by the boundary condition imposed by the former one. A similar expansion is made for $\mathbf{u_2}$ according to Eq. (51). Convergence and validation of the method will be demonstrated in Sec. III.

### D. Linear system

In order to apply the boundary conditions defined by Eq. (54), we truncate all our expansions in Eqs. (13)–(15) onto

$M+1$ angular ($\theta$) modes defined by $6M+3$ constants (the zeroth mode only adds 3 constants). Starting with a reflection $\mathbf{U}$ defined from one of the flagellum $C_{i-1}$, we compute the velocity boundary conditions onto the other flagellum $C_i$, which defines the new reflection $\mathbf{u}$. In order to match those two functions, we do a modal projection using the angular modes of the coordinate system in which the boundary condition is trivially defined by $r = kR$. Each projection on one mode gives us a $(6\times 6)$ linear system (except for the 0 mode that only adds 3 equations) such that $\mathcal{M}X = Y$, with noting $T$ the transpose

$$\mathcal{M} = \begin{pmatrix} \int_{C_i} u(r_i,\theta_i)\cos n\theta_i dS \\ \int_{C_i} v(r_i,\theta_i)\sin n\theta_i dS \\ \int_{C_i} w(r_i,\theta_i)\cos n\theta_i dS \\ \int_{C_i} u(r_i,\theta_i)\sin n\theta_i dS \\ \int_{C_i} v(r_i,\theta_i)\cos n\theta_i dS \\ \int_{C_i} w(r_i,\theta_i)\sin n\theta_i dS \end{pmatrix}, \tag{55}$$

$$Y = \begin{pmatrix} \int_{C_i} \mathbf{U}(r_{i-1},\theta_{i-1})\cdot\mathbf{e}_{\mathbf{r_i}}\cos n\theta_i dS \\ \int_{C_i} \mathbf{V}(r_{i-1},\theta_{i-1})\cdot\mathbf{e}_{\theta_\mathbf{i}}\sin n\theta_i dS \\ \int_{C_i} \mathbf{W}(r_{i-1},\theta_{i-1})\cdot\mathbf{e}_{\mathbf{z_i}}\cos n\theta_i dS \\ \int_{C_i} \mathbf{U}(r_{i-1},\theta_{i-1})\cdot\mathbf{e}_{\mathbf{r_i}}\sin n\theta_i dS \\ \int_{C_i} \mathbf{V}(r_{i-1},\theta_{i-1})\cdot\mathbf{e}_{\theta_\mathbf{i}}\cos n\theta_i dS \\ \int_{C_i} \mathbf{W}(r_{i-1},\theta_{i-1})\cdot\mathbf{e}_{\mathbf{z_i}}\sin n\theta_i dS \end{pmatrix}, \tag{56}$$

and

$$X = (A_n, C_n, D_n, B_n, E_n, F_n)^T. \tag{57}$$

Projecting onto the $M+1$ angular modes [$n$ ranges thus from 0 to $M$ in Eqs. (55)–(57)], we obtain a linear system of size $(6M+3)\times(6M+3)$. The matrix $\mathcal{M}$ can be inverted analytically as we compute the new reflection in the basis in which it is defined. However, the boundary condition $Y$ is not trivial to derive analytically, and we evaluate it in Matlab using adequate geometrical formulas for the change of coordinate systems from one cylindrical flagellum to the next. Once the new reflection has been computed, we proceed the same way on the other flagellum. We chose $M = 10$ angular modes in all our simulations, which appeared to be sufficient to approximate our boundary conditions, and leave our results unchanged upon a change of the number of modes.

### E. Rate of energy dissipation

Once the linear system is solved, we have access to the pressure and velocity fields. The dimensionless rate of energy dissipation per unit length per second is given by

$$W = \frac{1}{2\pi}\int_s\int_\theta \boldsymbol{\sigma}\cdot\mathbf{u}\cdot(-\mathbf{n})d\theta ds. \tag{58}$$

That is, noting $\mathbf{u} = U\mathbf{e_r} + V\mathbf{e}_\theta$, we get

$$W = \frac{1}{2\pi}\int_s\int_\theta -\sigma_{rr}U - \sigma_{r\theta}V d\theta ds, \tag{59}$$

$$\sigma_{rr} = -p + \frac{\partial u}{\partial r}, \tag{60}$$

$$\sigma_{r\theta} = \frac{\partial v}{\partial r} - \frac{v}{r} + \frac{1}{r}\frac{\partial u}{\partial \theta}. \tag{61}$$

On each of our flagella, the velocity components at order $(bk)$ are given for all $\theta$ by Eqs. (38)–(40), so that we have on the flagellum

$$-\frac{v}{r} + \frac{1}{r}\frac{\partial u}{\partial\theta} = 0. \tag{62}$$

Furthermore, using the continuity equation, Eq. (12), combined with our boundary condition on $w$, we get

$$\frac{\partial w}{\partial z} = \frac{\partial u}{\partial r} + \frac{u}{r} + \frac{1}{r}\frac{\partial v}{\partial\theta} = \frac{\partial u}{\partial r} = 0. \tag{63}$$

The stress tensor on the cylindrical filaments reduces thus to

$$\sigma_{rr} = -p, \tag{64}$$

$$\sigma_{r\theta} = \frac{\partial v}{\partial r}, \tag{65}$$

so that

$$\begin{aligned} 2\pi W = {} & \cos\phi\cos\beta\int_s\int_\theta p\cos\theta\cos s \\ & + \cos\phi\sin\beta\int_s\int_\theta p\sin\theta\cos s \\ & + \cos\phi\cos\beta\int_s\int_\theta \frac{\partial v}{\partial r}\sin\theta\cos s \\ & - \cos\phi\sin\beta\int_s\int_\theta \frac{\partial v}{\partial r}\cos\theta\cos s. \end{aligned} \tag{66}$$

Note that since the leading order flow is at order $(kb)$, the leading order viscous dissipation occurs at order $(kb)^2$. To evaluate the portion of Eq. (66) on each flagellum, we have to express the terms defined from the other flagellum into the current coordinate system. This is simply done using crossed derivative formulas. Interestingly enough, only the first mode defined from the current flagellum will play a role in the computation of the rate of energy dissipation on this flagellum.

## III. TWO BEATING FLAGELLAS

We consider in this section the beating of two cylindrical flagella. After validating our implementation of the reflection method, we address the situation where both flagella beat in their plane of separation and show that in this case the results are similar to Taylor's previous work in two dimensions. We next investigate out-of-plane beating and compute the sets of orientations minimizing the rate of energy dissipation. Our results are then illustrated using a simple model of two periodically translating spheres interacting hydrodynamically in the far field.

### A. Setup and validation

In order to validate our reflection method, we first verify that we do indeed match the boundary conditions on each of the two flagella. The matching is illustrated in Fig. 2, where we plot the angular dependence of both components of the prescribed ($U$) and computed ($u$) on the cylinder $C_1$, as well as the dimensionless relative error, $(U-u)/U$, between the two.

We then analyze the convergence of the reflection method with the distance between the two flagella. We observe uniform convergence of the reflections toward zero. Numerically, we stop implementing new reflections when adding one improves

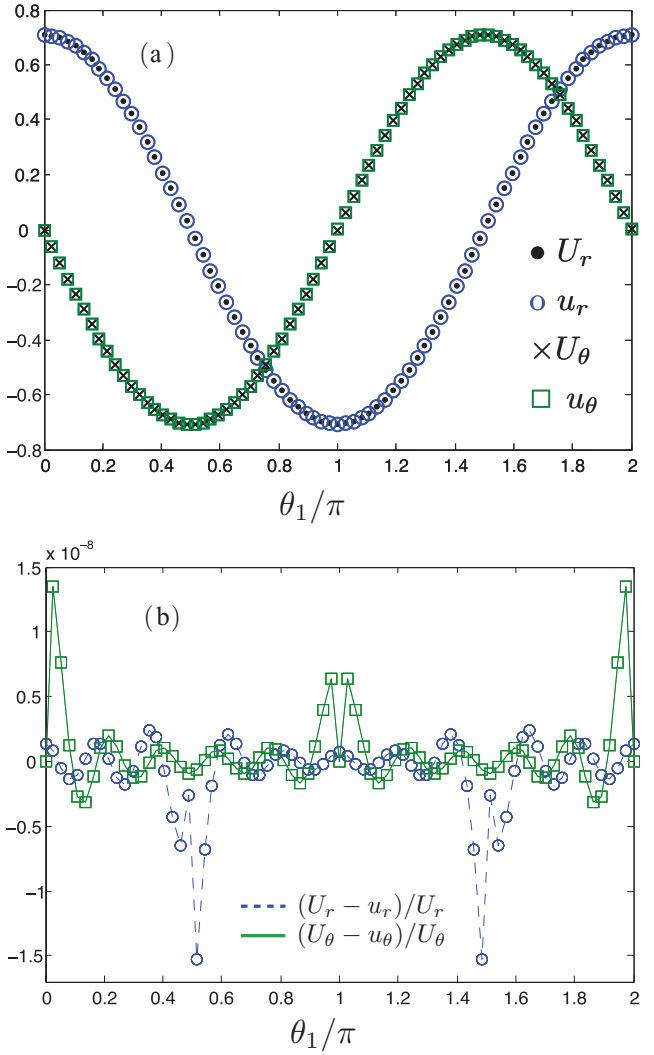


FIG. 2. (Color online) (a) Matching on the cylinder $C_1$ of the prescribed $(U_r, U_\theta)$ and computed $(u_r, u_\theta)$ radial and tangential components of the velocity for the parameters: $a = 5R$, $kR = 10^{-2}$, $s = 0$, and $\phi = \pi/4$. The $w$ component is found to be equal to zero within Matlab's precision. (b) Angular dependence of the dimensionless relative error, $(U - u)/U$, between the prescribed and computed velocity components (blue dashed line, $u_r$; green solid line, $u_\theta$).

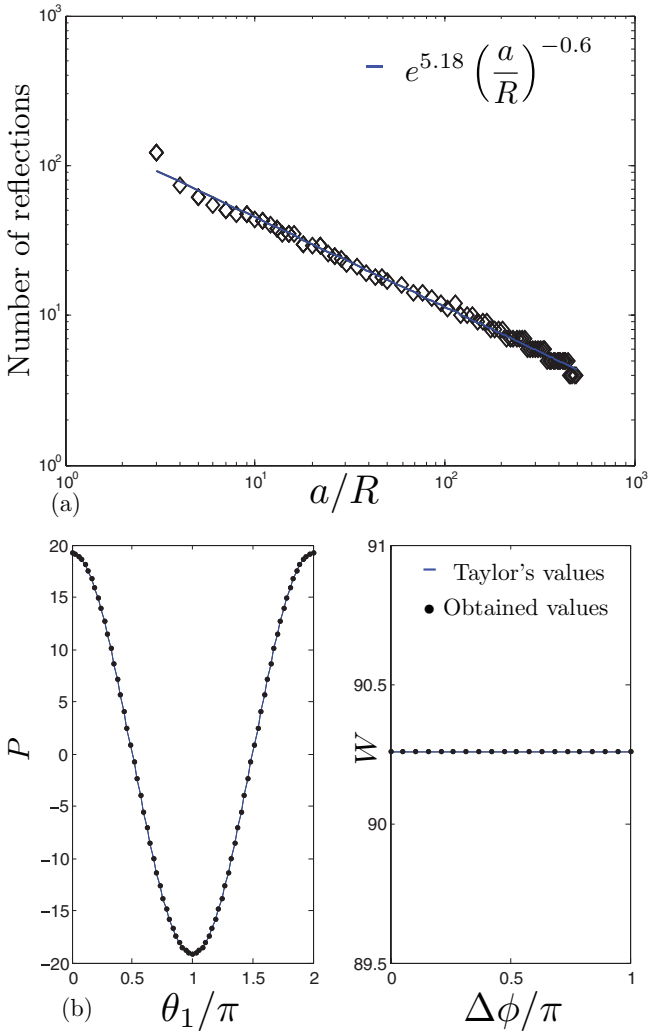


FIG. 3. (Color online) (a) Number of reflections needed as a function of the distance between the flagella for $kR = 0.01$ (log-log scale). (b) Matching between Taylor's pressure field evaluated on $C_1$ (solid line, left) and energy dissipation rate (right) and our results (dots) for the parameters: $R = 1$, $k = 0.01$, and $a/R = 10^4$.

the matching of the three components of the boundary conditions by less then 1%. The dependence of the number of necessary reflections as a function of the average distance between the beating flagella is shown in Fig. 3(a). As expected, the further the flagella, the weaker the hydrodynamic interactions, and the faster the reflection method is converging. Our rate of convergence is well fitted by a power-law.

Since the interactions between the two flagella disappear in the limit where their separation distance becomes infinite, we verify that Taylor's result for the individual beating of three-dimensional flagella [35] is recovered in this limit. This matching is shown in Fig. 3(b) for the pressure field on the cylinder $C_1$ and the rate of energy dissipation. As expected, the rate of energy dissipation is independent of the phase difference $\Delta\phi$ between the flagella in this limit.

### B. In-plane beating

In order to extend Taylor's work, we first analyze the case of in-plane beating corresponding to $\beta_1 = \beta_2 = 0$. Instantaneous snapshots of the pressure, flow, and vorticity fields are shown in Fig. 4 for representative values of our main geometrical parameters (the value of $s$ is chosen so that the flow field is not zero in the three examples shown), and three values of the phase difference $\Delta\phi$: 0, $\pi/2$, and $\pi$.

The dependence of the rate of energy dissipation on the phase difference is displayed in Fig. 5 (top) for various values of the dimensionless distance between the flagella, $a/R$. We observe that the minimum $W_{\min}$ corresponds to the case where the two flagella beat in phase ($\Delta\phi = 0\,[2\pi]$), similar to Taylor's two-dimensional results. The maximum $W_{\max}$ occurs when the two flagella beat in opposition of phase ($\Delta\phi = \pi\,[2\pi]$).

In addition, we note that $W_{\min}$ decreases when the distance between the flagellar filaments decreases, meaning that the

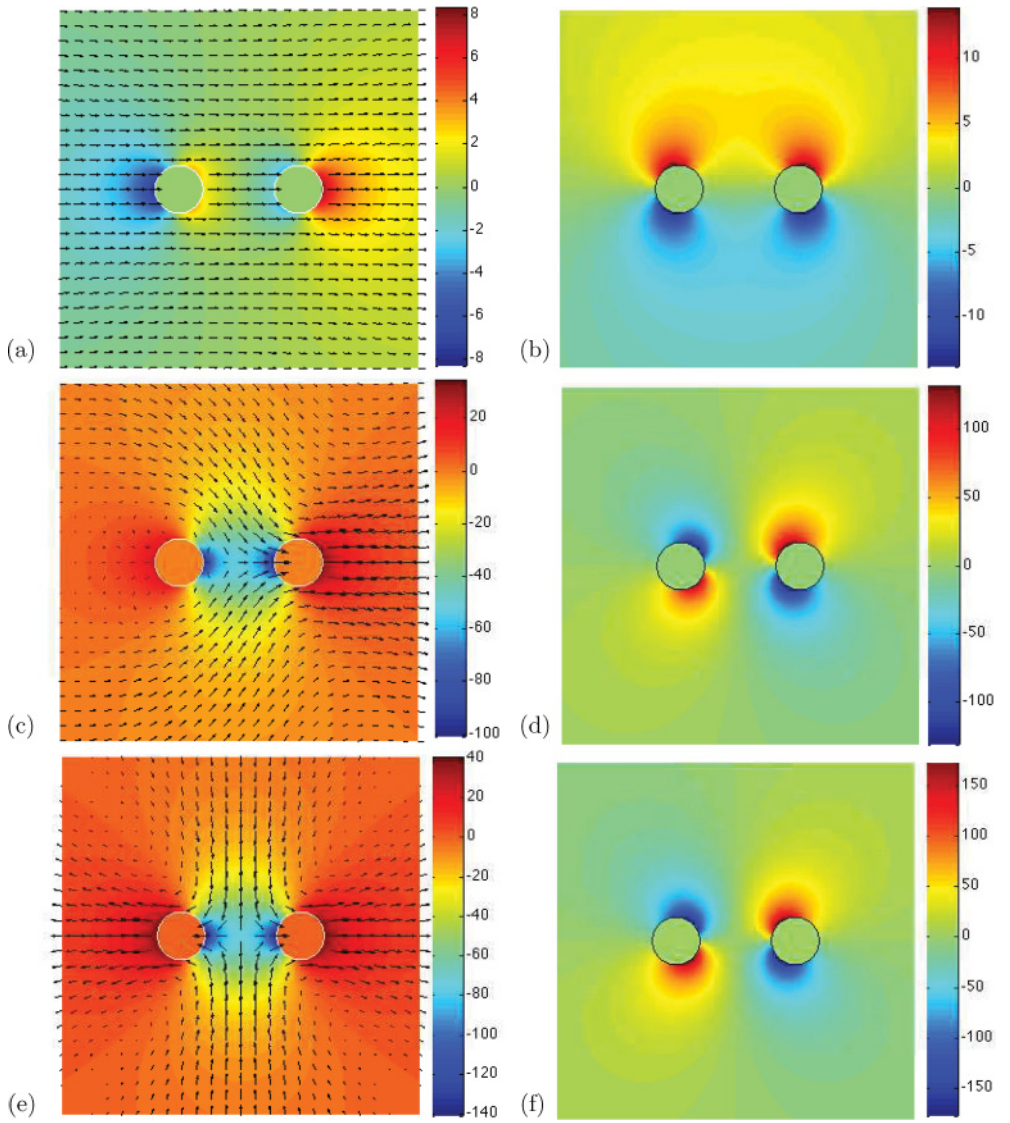


FIG. 4. (Color online) Instantaneous velocity and pressure fields (left) and $z$ component of the vorticity (right) for the in-plane beating of two flagella, with $ka = kb = 0.05$, $R = 1$, $s = 1$, and the following values of the phase differences: $\Delta\phi = 0$ (a, b), $\Delta\phi = \pi/2$ (c, d), and $\Delta\phi = \pi$ (e, f).

optimal situation from an energy standpoint is close in-phase swimming. The dependence of the ratio of $W_{\min}/W_{\max}$ with the distance between the flagella is displayed in Fig. 5 (bottom), together with Taylor's qualitatively similar results in two dimensions [31].

### C. Out-of-plane beating

We now consider the more general case, where the beating of the flagella does not take place in the plane defined by their axis, and thus $\beta_1$ and $\beta_2$ can take nonzero values. Given all possible phase differences between the flagella, by symmetry it is sufficient to consider orientations in the interval $\beta_1 \in [0,\pi]$ to recover all possible cases.

To obtain the optimal phase configuration, we first fix the value of the beating orientation $\beta_1$ of $C_1$ and compute the rate of energy dissipation for all possible values of $\beta_2$ and $\Delta\phi$. We then determine numerically, for each value of $\beta_2$, the optimal phase difference $\Delta\phi$ leading to the smallest and largest values of $W$. The map of the optimal phase difference $\Delta\phi$ as a function of the set of orientations $(\beta_1,\beta_2)$ is displayed in Fig. 6.

Our main result is that, for all configurations, the phase difference $\Delta\phi$ leading to the minimum of the rate of energy dissipation is always either 0 or $\pi$ (modulo $2\pi$), while the one leading to a maximum is always either $\pi$ or 0. In Fig. 6 we plot an empirical curve, obtained numerically, separating these two optimal domains for different values of the distance between the flagella. Note that, surprisingly, for the case $\beta_1 = \pi/2$ and $\beta_2 = 0$ (and inversely) we find that the energy dissipation rate is independent of the phase difference between the flagella (not shown).

For a given value of $\beta_1$, we can then define the optimal $\beta_2$ as the one that minimizes the energy dissipation rate, namely

$$W^{\text{opt}}\left(\beta_2^{\text{opt}},\Delta\phi^{\text{opt}}\right)|_{\beta_1} = \min_{\beta_2,\Delta\phi} W(\beta_2,\Delta\phi)|_{\beta_1}\,. \qquad (67)$$

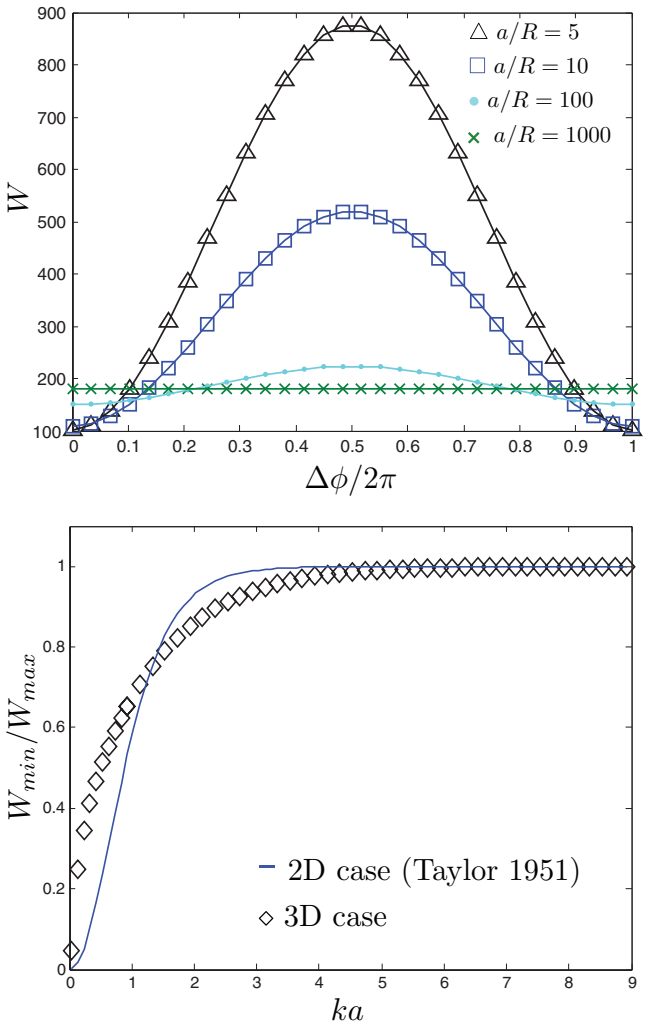


FIG. 5. (Color online) Top: Dependence of the rate of energy dissipation, $W$, on the phase difference between the two flagella, $\Delta\phi$, for different values of the flagellum-flagellum distance $a/R$ and $kR = 0.01$. Bottom: Variation of the ratio of the minimum to the maximum of the rate of energy dissipation with $ka$ (symbols). The solid line displays Taylor's waving sheet results [31].

The results are displayed in Fig. 7 where we plot the optimal value $\beta_2^{\text{opt}}$ as a function of $\beta_1$ [Fig. 7(a)] and the corresponding values of the energy dissipation rate [Fig. 7(b)]. Our main result here is that the overall optimal beating from an energy standpoint is always the in-plane beating, and any other orientation systematically lead to an increase of the viscous dissipation. We also obtain that, the closer the flagella, the lower the minimum rate of energy dissipation. As a difference, the worst case from an energy (minimum) standpoint is when the swimmers swim parallel to each other, both being perpendicular to their separation plane.

For the particular cases $\beta_1 = 0$ or $\beta_1 = \pi/2$, the optimal orientation for the second flagellum is given by $\beta_2 = \beta_1$. For the other orientations, we observe that the optimal case is close to $\beta_2 \approx \beta_1$, when the flagella are close to each other, indicating that parallel beating is always preferable in this case; this is no longer the case as the flagella get further apart.

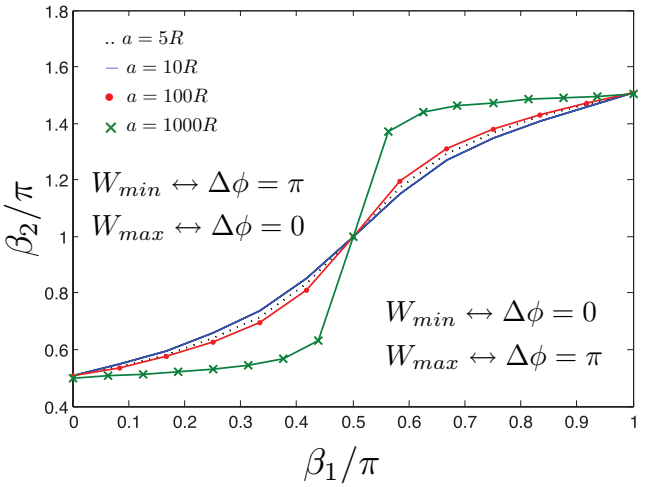


FIG. 6. (Color online) Map of the optimal phase difference between the flagella in the orientation space for $kR = 0.01$ and different dimensionless distances $a/R$. Each solid line splits the figure into two parts; In the upper part the rate of energy dissipation is found to be minimum for $\Delta\phi = \pi$ and maximum for $\Delta\phi = 0$, whereas in the lower part the minimum is obtained for $\Delta\phi = 0$ and the maximum for $\Delta\phi = \pi$.

### D. Simple model: Far-field interactions between two beating spheres

In order to further illustrate the dependency shown in Fig. 7(a), we put forward in this section a simple model consisting of two beating spheres. Assuming the spheres to be far from each other, we use the far-field approximation for hydrodynamic interactions in Stokes flow to compute the rate of energy dissipation as a function of the phase difference and orientations of the spheres.

We consider two periodically translating spheres (radius $R$), beating with orientations $\beta_1$ and $\beta_2$, and separated by distance $a$. The sphere motion is governed by a sinusoidal motion with the same geometrical parameters as the one previously defined for our flagella (see Fig. 1). In cartesian coordinates, the dimensionless velocities on the spheres are thus given by

$$\mathbf{U}_{\mathbf{S_1}} = \cos(kUt + \phi)(\cos\beta_1\mathbf{e_x} + \sin\beta_1\mathbf{e_y}), \tag{68}$$

$$\mathbf{U}_{\mathbf{S_2}} = \cos(kUt - \phi)(\cos\beta_2\mathbf{e_x} + \sin\beta_2\mathbf{e_y}). \tag{69}$$

We compute the rate of energy dissipation per unit period, $W_{S_1}$, on the sphere $S_1$; the formula for the sphere $S_2$ is obtained using symmetry by a $1 \leftrightarrow 2$ permutation on the indices. In the case of two flagella, we integrate along the $z$ axis so as to take into account the motion over a whole period. The equivalent here consists in integrating over a period of time $T$. We therefore have

$$W_{S_1} = \frac{1}{T}\int_0^T \int_{S_1} \boldsymbol{\sigma}\cdot\mathbf{U}_{\mathbf{S_1}}\cdot(-\mathbf{n})\,dS\,dt. \tag{70}$$

Since the spheres undergo rigid-body motion, we have

$$\int_{S_1} \boldsymbol{\sigma}\cdot\mathbf{U}_{\mathbf{S_1}}\cdot(-\mathbf{n})\,dS = -\mathbf{U}_{\mathbf{S_1}}\cdot\mathbf{F}_{\mathbf{S_1}}, \tag{71}$$

where $\mathbf{F}_{\mathbf{S_1}}$ is the force exerted by the fluid on the sphere $S_1$.

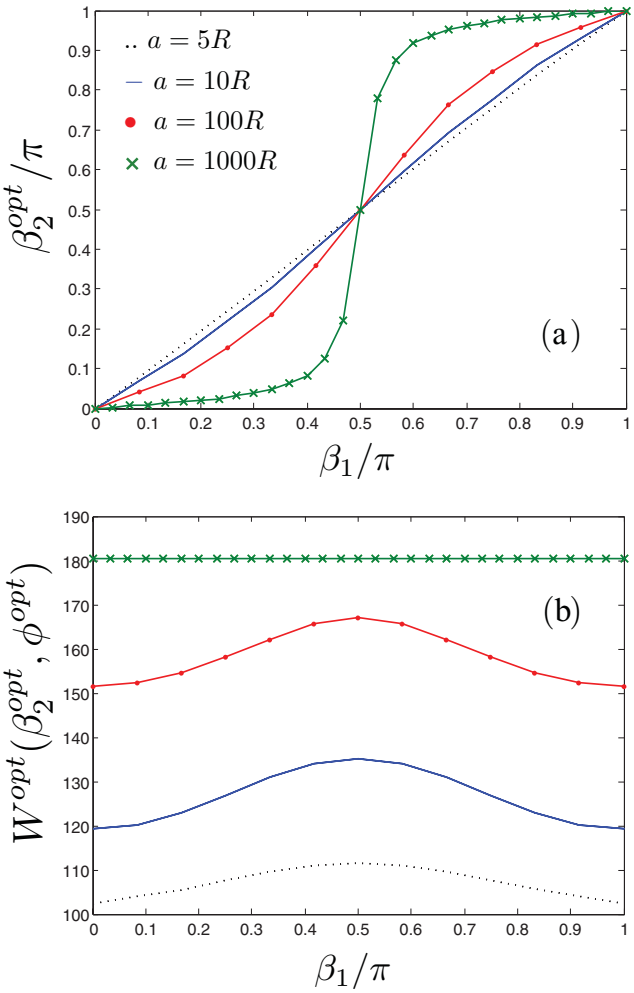


FIG. 7. (Color online) (a) Orientations pairs leading to the minimum of the rate of energy dissipation as defined in Eq. (67), for various dimensionless distances, $a/R$. (b) Corresponding values of the optimal rate of energy dissipation for each of these pairs. In both figures, we have $kR = 0.01$.

In the far-field limit ($R/a \ll 1$), we can approximate the velocity fields using the first order monopole (Stokleslet) expansion [22,60]:

$$\mathbf{F}_{\mathbf{S}_1} = \mathbf{F}^{\mathbf{0}}_{\mathbf{S}_1} + \mathbf{F}^{\mathbf{1}}_{\mathbf{S}_1}, \tag{72}$$

$$\mathbf{F}^{\mathbf{0}}_{\mathbf{S}_1} = -6\pi \mathbf{U}_{\mathbf{S}_1}, \tag{73}$$

$$\mathbf{F}^{\mathbf{1}}_{\mathbf{S}_1} = \mathbf{F}^{\mathbf{0}}_{\mathbf{S}_2}\left[-\frac{3R}{2a}\mathbf{dd} - \frac{3R}{4a}(\boldsymbol{\delta} - \mathbf{dd})\right], \tag{74}$$

where $\mathbf{d}$ is the vector joining $S_1$ to $S_2$, and $\boldsymbol{\delta}$ the identity tensor. To the first order in the beating amplitude the spheres are immobile so that we have

$$\mathbf{d} = \frac{\mathbf{x_2} - \mathbf{x_1}}{|\mathbf{x_2} - \mathbf{x_1}|} = \mathbf{e_x}, \tag{75}$$

$$\mathbf{F}^{\mathbf{1}}_{\mathbf{S}_1} = -\frac{3R}{2a}\mathbf{F}^{\mathbf{0}}_{\mathbf{S}_2} \cdot \mathbf{e_x}\mathbf{e_x} - \frac{3R}{4a}\mathbf{F}^{\mathbf{0}}_{\mathbf{S}_2} \cdot \mathbf{e_y}\mathbf{e_y}, \tag{76}$$

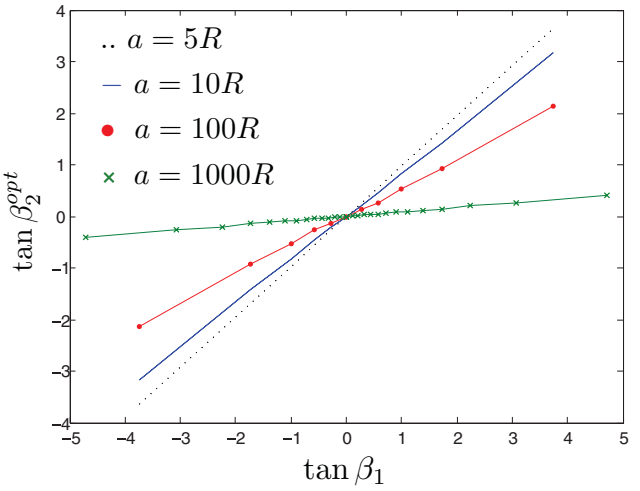


FIG. 8. (Color online) Flagella orientations pairs leading to the minimum rate of energy dissipation. The data from Fig. 7(a) are replotted using the tangent function. We recover an almost linear relationship, similar to the case of two spheres in the far field [Eq. (83)]. $kR = 0.01$.

where $\mathbf{x_1}$ and $\mathbf{x_2}$ are the position of the centers of, respectively, $S_1$ and $S_2$. The total rate of energy dissipation between the two spheres is given by

$$W = -\int_0^1 \left(\mathbf{U}_{\mathbf{S}_1} \cdot \mathbf{F}_{\mathbf{S}_1} + \mathbf{U}_{\mathbf{S}_2} \cdot \mathbf{F}_{\mathbf{S}_2}\right) dt, \tag{77}$$

so that

$$\frac{W}{6\pi} = \int_0^1 \left[|\mathbf{U}_{\mathbf{S}_1}|^2 + |\mathbf{U}_{\mathbf{S}_2}|^2 - \frac{3R}{a}(\mathbf{U}_{\mathbf{S}_1} \cdot \mathbf{e_x})(\mathbf{U}_{\mathbf{S}_2} \cdot \mathbf{e_x}) - \frac{3R}{2a}(\mathbf{U}_{\mathbf{S}_1} \cdot \mathbf{e_y})(\mathbf{U}_{\mathbf{S}_2} \cdot \mathbf{e_y})\right] dt. \tag{78}$$

After some algebra we get

$$\frac{W}{6\pi} = 1 - \frac{3R}{2a}\cos 2\phi \left[\cos\beta_1 \cos\beta_2 + \frac{1}{2}\sin\beta_1 \sin\beta_2\right]. \tag{79}$$

Equation (79) shows several properties similar to our flagella results. First, we recover that for $\beta_1 = \pi/2$ and $\beta_2 = 0$ (or vice-versa), the rate of energy dissipation does not depend on the phase difference between the spheres. Second, for fixed orientations, the optimal phase difference is obtained for $\partial W/\partial\phi = 0$, which is achieved for

$$\sin 2\phi \left[\cos\beta_1 \cos\beta_2 + \frac{1}{2}\sin\beta_1 \sin\beta_2\right] = 0. \tag{80}$$

The extremum are thus found to be $\Delta\phi = 2\phi = 0$ and $\pi$, similarly to our results for two flagella. Third, for a given orientation of $S_1$, the optimal orientation $\beta_2$ is such that

$$\frac{\partial W}{\partial \beta_2}|_{\beta_1} = 0, \tag{81}$$

leading to

$$2\cos\beta_1 \sin\beta_2^{\text{opt}} = \sin\beta_1 \cos\beta_2^{\text{opt}}. \tag{82}$$

From Eq. (82) we get that the extremum is $\beta_2^{\text{opt}} = \beta_1$ in the particular cases $\beta_1 = 0$ and $\beta_1 = \frac{\pi}{2}$, while for any other value of $\beta_1$ we obtain an optimal value analytically as

$$\tan \beta_2^{\text{opt}} = \frac{1}{2} \tan \beta_1. \tag{83}$$

Inspired by the analytical result of Eq. (83), we replot the data of Fig. 7(a) using, not the orientation angles themselves, but the tangent of the angles, and the result is shown in Fig. 8. Seemingly for all values of the dimensionless distance between the flagella $a/R$, we obtain a near linear relationship between $\tan \beta_2^{\text{opt}}$ and $\tan \beta_1$. For our value of $kR$ (0.01), the slope of the linear relation is only a function of $a/R$. All of the essential physics of the energetics for synchronized states of a pair of flagella is thus recovered by this simple problem of two spheres.

## IV. THREE BEATING FLAGELLA

Since the Stokes equations are linear, it is straightforward to extend our reflection method to study a situation with more than two flagella. We address in this section the three-flagella case. We first detail the parametrization of the problem, the implementation of the reflection method, and its validation. We then present examples of the flow field and of the rate of energy dissipation for two configurations.

### A. Procedure and numerical validation

We use the same parametrization as the one used in the two-flagella case and designate our three cylinders by $C_1$, $C_2$, and $C_3$. The flagella are deformed by a sinusoidal wave, similar to Sec. II. We assume for simplicity that all three flagella beat in the same direction with $\beta_1 = \beta_2 = \beta_3 = 0$, and we take $kR = 0.01$.

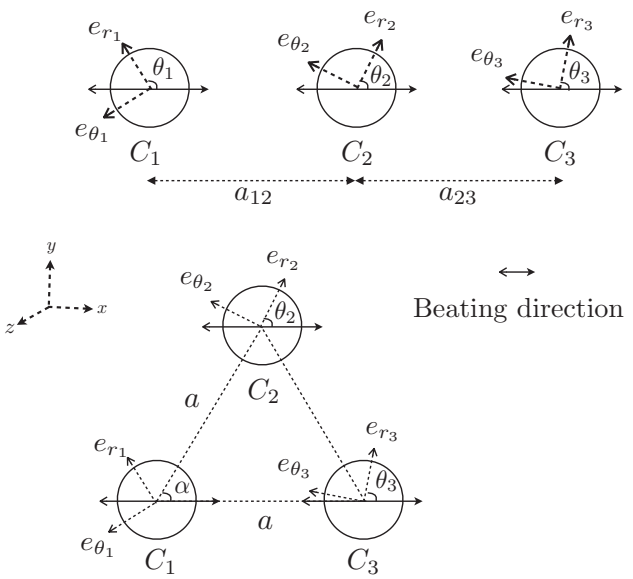


FIG. 9. Two configurations of three beating flagella, with notations. Top: aligned case; bottom: triangular case. In both configurations we assume in-plane beating.

Since we have a third flagellum, we now have to take into account two relative phase differences, namely the difference between $C_1$ and $C_2$, and the difference between $C_1$ and $C_3$. To do so, we impose without loss of generality $\phi_1 = 0$ and take independently $(\phi_2, \phi_3)$ in $[0, \pi]^2$. The boundary conditions are the same as the ones previously derived, provided that we use the adequate parameters and indices for each cylinder. We propose here to study two specific configurations, one where all three flagella are aligned and one where they are located at the edge of an equilateral triangle, as shown in Fig. 9.

We implement the reflection method iteratively as follows. We start by summing up all the reflection terms defined from $C_1$ that have not yet been matched and compute the associated reflections on the other two flagella. We then repeat for the flagella $C_2$ and $C_3$ and iterate until additional iterations only improves the matching of each boundary conditions by less

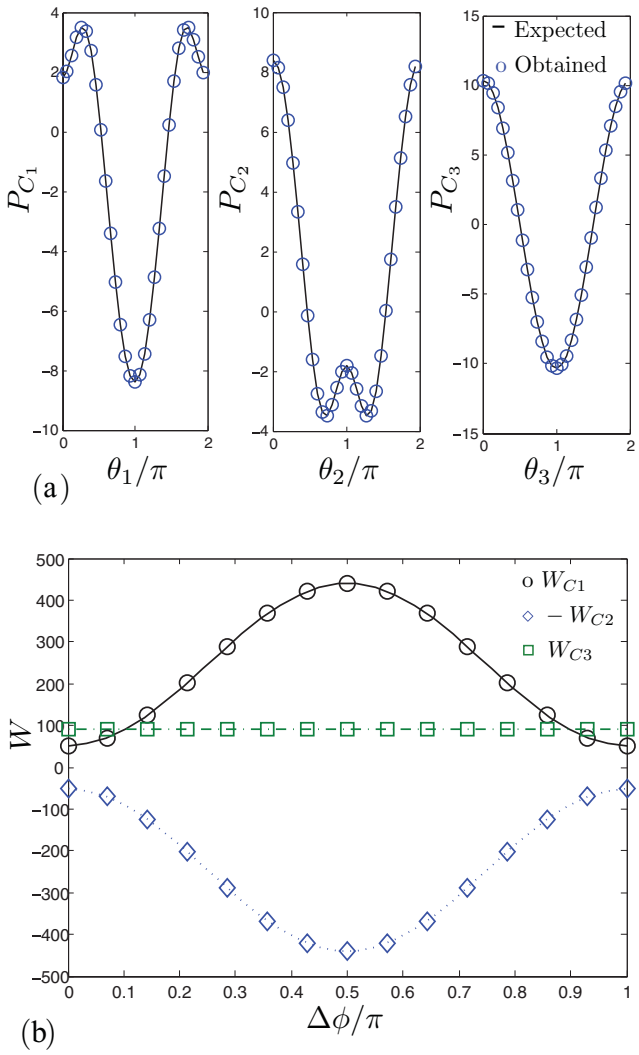


FIG. 10. (Color online) Numerical validation of the reflection method in the case of three aligned flagella for $a_{12}/R = 5$, $a_{23}/R = 10^4$, and $kR = 0.01$; (a) Pressure distribution around each cylinder; (b) rate of viscous dissipation. Numerical results using the three-flagella reflection method are shown using symbols, while the expected results are shown using lines.

TABLE I. Relative variation of the minimum rate of energy dissipation. $n$ corresponds to the number of flagella considered, and $W_j$ (with $j = 1,n$) is the rate of work for $j$ filaments.

| | Individual | 2 flagella | 3 flagella, aligned | 3 flagella, triangle |
|---|---|---|---|---|
| $W_n$ | $W_1 = 90.257$ | $W_2 = 102.29$ | $W_3 = 112.562$ | $W_3 = 114.994$ |
| $(nW_1 - W_n)/nW_1$ | | 43.3% | 58.4% | 57.5% |

then 1%. Our method essentially involves thus an iterative calculation of two-flagella interactions for each of the three-flagella pairs.

After matching the boundary conditions on our flagella, we choose the aligned case to validate the method and its implementation. We put $C_1$ and $C_2$ at a distance $a_{12}/R = 5$ from each other and $C_3$ to a distance $a_{23}/R = 10^4$ from $C_2$. We then check that we recover both our former two-flagella results for the pressure and rate of energy dissipation on $C_1$ and $C_2$ and Taylor's results for individual swimmer on $C_3$. This validation is shown in Fig. 10.

### B. Aligned and triangular configurations

We present here examples of the flow field and rate of energy dissipation for the two particular configurations depicted in Fig. 9. The first configuration corresponds to the case were the three flagella beat in the same plane, each at a dimensionless distance $a/R = 5$ from their nearest neighbor, and the second one to the case where the three flagella form an equilateral triangular configuration of dimensionless edge length $a/R = 5$. Instantaneous snapshots of the velocity and pressure fields are shown in Fig. 11 (left, aligned configuration; right, triangular case).

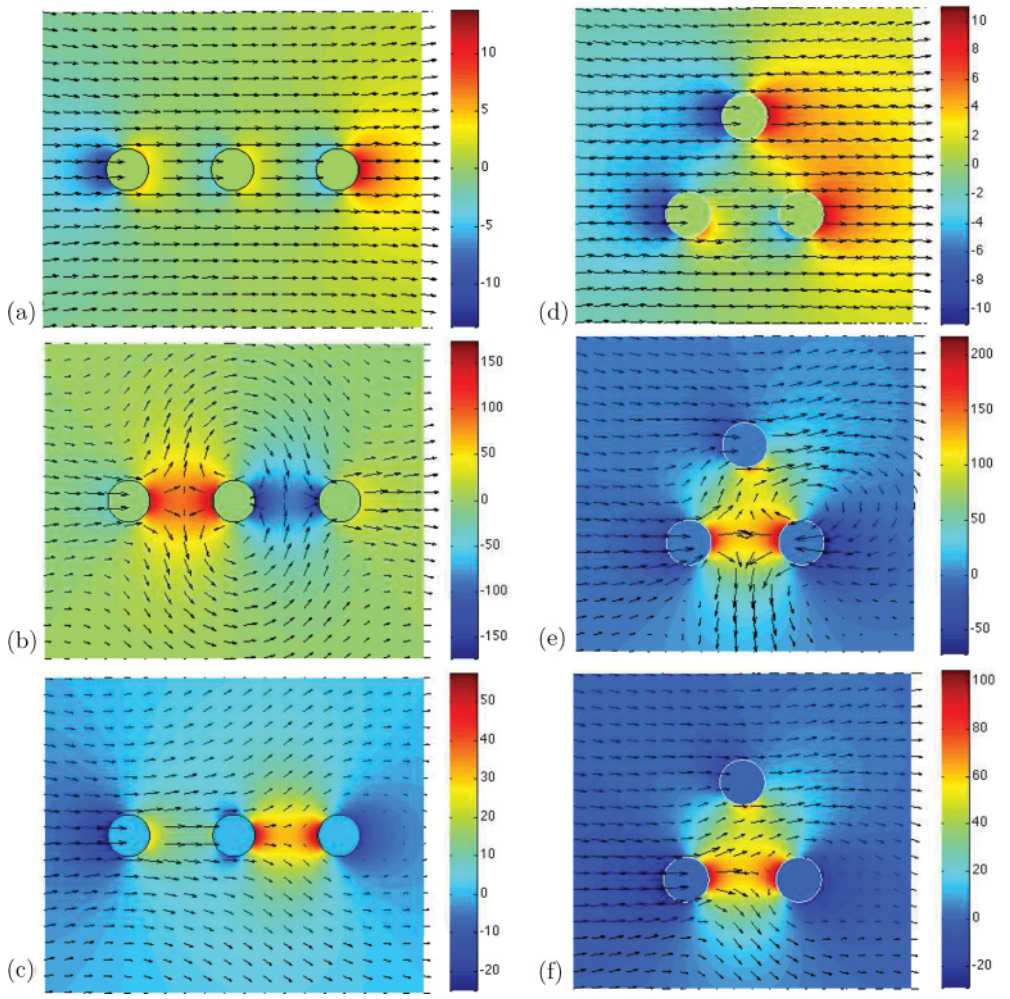


FIG. 11. (Color online) Instantaneous velocity and pressure fields for the in-plane beating of three aligned flagella (left) and triangular configuration (right). The relative phase differences are (a, d) $\phi_2 = \phi_3 = 0$; (b, e) $\phi_2 = \pi, \phi_3 = 0$; (c, f) $\phi_2 = \pi/4, \phi_3 = \pi/2$, and the plots are displayed for $s = 0$ and $kR = 0.01$.

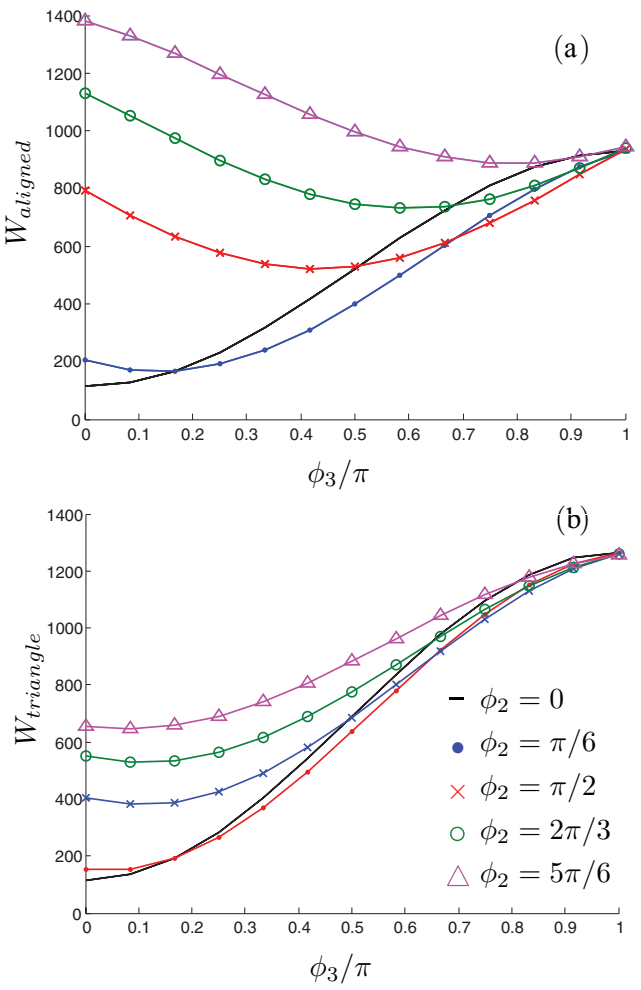


FIG. 12. (Color online) Evolution of the rate of energy dissipation with $\phi_3$ for different values of $\phi_2$. (a) Aligned configuration; (b) triangular configuration.

The variation of the rate of viscous dissipation with the two relative phase differences is displayed in Fig. 12 for these two configurations. In both cases, the minimum is still obtained for in-phase beating of all three flagella. Aligned in-phase swimming is found to be more efficient then triangular swimming. In the aligned configuration, the dissipated energy is found to be maximum for $\phi_2 = \pi, \phi_3 = 0$, whereas for the triangular configuration the maximum is obtained for $\phi_2 = 0, \phi_3 = \pi$. Our numerical results for the minimum energy are summarized in Table I, where we also give the relative reduction of minimum dissipated energy compared to the individual swimming case in order to quantify the efficiency of collective swimming. This is quantified by the dimensionless difference between the rate of work of $n$ individual flagella, $nW_1$, and that of a $n$-flagella configuration, $W_n$. The dimensionless reduction of work is observed to be larger for three flagella than two, indicating an increased efficiency of collective beating with the number of flagella.

## V. CONCLUSION

The flow field and energetics induced by the small-amplitude beating of two or three infinite flagella of cylindrical cross section was studied using a semianalytical method based on the method of reflections. In the case of two flagella, we first extended Taylor's work [31] to three dimensions and showed that the rate of energy dissipation is still minimum for in-phase beating and maximum for out-of-phase beating when the flagella are beating in the same plane as the one defined by their axis. The dependence of the ratio between the minimum and the maximum rate of energy dissipation with the distance between the flagella was found to be qualitatively similar to the one computed by Taylor in his two-dimensional model [31], and the larger energetic gain is obtained for in-phase beating of nearby flagella.

When allowing the flagellar filaments to beat in any direction, we found that the minimum energy dissipation rate occurs either for in-phase or opposite-phase beating, depending on the beating orientations, $\beta_1$ and $\beta_2$, and the distance between the flagella. We then characterized the optimal orientation pairs by searching, for each value of $\beta_1$, the $\beta_2$ minimizing the energy dissipation rate over all possible phase differences.

For the particular cases $\beta_1 = 0$ or $\pi/2$, the minimum is reached for $\beta_2 = \beta_1$. For an orthogonal conformation, the rate of energy dissipation was observed to be independent of the phase difference between the two flagella. For all other cases, the variation of the optimal orientation pairs follows a law of the form $\tan\beta_2 = A\tan\beta_1$, where $A$ is a constant that depends on the distance between the flagella and which tends to one when the flagella are located near one another (so that the optimal orientations beating in close proximity are the parallel ones). The overall lowest rate of energy dissipation is obtained for in-plane in-phase beating.

We then illustrated our flagella results using a simple model of two beating spheres interacting hydrodynamically in the far field. The dissipation rate, which, with this model, can be computed analytically, gives essentially the same results as the ones obtained for the beating flagella, thereby providing us with a simple physical model for three-dimensional flagella beating.

Exploiting the linearity of the Stokes equations, we then used an extension of our method to address the case of three beating flagella, in two configurations: one aligned and one where the flagella are located at the edges of a triangle. Here again the beating modes leading to the minimum rate of energy dissipation were obtained to be in-phase waving motion for all three flagella. In addition, a comparison between the beating of one, two, and three flagella showed an increased efficiency of collective beating with the number of nearby filaments.

As was observed experimentally, swimming spermatozoa have a tendency to form a bundle, their beating filaments synchronizing with the beating of their neighbors, resulting in an increased efficiency of swimming compared to individual cells [36–38]. Our results, in line with Taylor's seminal work in two dimensions, suggest that from a hydrodynamic point of view, it is more energetically efficient for spermatozoa with three-dimensional flagella to swim close to each other and with synchronized in-phase beating.

The major modeling assumptions in our paper were the restriction to the small-amplitude beating of infinite filaments. Our group recently devised a method to extend Taylor's small-amplitude perturbation expansion to large wave

amplitudes, and this method could in theory be applicable here [61]. Computationally, large amplitude waves on sheets were addressed in Ref. [52], with results very similar to Taylor's, and therefore our results will probably remain valid in the large-amplitude limit. The case of finite swimmers was addressed in Ref. [53], which computed the synchronization dynamics for two-dimensional sheet-like swimmers displaying about one-and-a-half wavelengths (compared to Taylor's infinite wave geometry). Here again, the rate of working by the swimmers is minimum for in-phase swimming, and end effects do not change Taylor's results qualitatively, provided the swimmers are parallel to each other.

In regards to biological modeling, the logical next step in our approach would consist, instead of prescribing the shapes of the flagellar waves, in specifying the internal molecular forcing at the level of the axoneme [62,63] and then computing the resulting flagellar shapes and dynamics. A preliminary two-dimensional model shows that flow-induced deformations will always dynamically lead to a synchronized in-phase conformation of two flexible internally forced sheets [56]. The extension of these results to three dimensions would provide further modeling insight in the collective dynamics of flagellated cells.

## ACKNOWLEDGMENTS

We thank Saverio Spagnolie, Gwynn Elfring, and Tony Davis for useful discussions. This work was supported in part by the National Science Foundation (Grant No. CBET-0746285 to E.L.).

[1] J. Gray, *Animal Locomotion* (Norton, London, 1968).
[2] R. M. Alexander, *Principles of Animal Locomotion* (Princeton University Press, Princeton, 2002).
[3] D. Bray, *Cell Movements* (Garland Publishing, New York, 2000).
[4] L. J. Fauci and R. Dillon, Annu. Rev. Fluid Mech. **38**, 371 (2006).
[5] E. Lauga and T. R. Powers, Rep. Prog. Phys. **72**, 096601 (2009).
[6] S. S. Suarez and A. A. Pacey, Hum. Reprod. Update **12**, 23 (2006).
[7] H. C. Berg, *E.coli in Motion* (Springer, New York, 2004).
[8] J. O. Kessler, Contemp. Phys. **26**, 147 (1985).
[9] R. H. Luchsinger, B. Bergersen, and J. G. Mitchell, Biophys. J. **77**, 2377 (1999).
[10] R. Dreyfus, J. Baudry, M. L. Roper, M. Fermigier, H. A. Stone, and J. Bibette, Nature (London) **437**, 862 (2005).
[11] A. Ghosh and P. Fischer, Nano Lett. **9**, 2243 (2009).
[12] L. Zhang, J. J. Abbott, L. Dong, B. E. Kratochvil, D. Bell, and B. J. Nelson, Appl. Phys. Lett. **94**, 064107 (2009).
[13] L. Zhang, J. J. Abbott, L. Dong, K. E. Peyer, B. E. Kratochvil, H. Zhang, C. Bergeles, and B. J. Nelson, Nano Lett. **9**, 3663 (2009).
[14] W. Gao, S. Sattayasamitsathit, K. M. Manesh, D. Weihs, and J. Wang, J. Am. Chem. Soc. **132**, 14403 (2010).
[15] J. Wang, ACS Nano **3**, 4 (2009).
[16] B. J. Nelson, I. K. Kaliakatsos, and J. J. Abbott, Annu. Rev. Biomed. Eng. **12**, 55 (2010).
[17] M. J. Kim and K. S. Breuer, Phys. Fluids **16**, L78 (2004).
[18] O. Tabata, H. Hirasawa, S. Aoki, R. Yoshida, and E. Kokufuta, Sensors and Actuators A **95** 234 (2002).
[19] D. B. Weibel, P. Garstecki, D. Ryan, W. R. Diluzio, M. Mayer, J. E. Seto, and G. M. Whitesides, Proc. Natl. Acad. Sci. USA **102**, 11963 (2005).
[20] A. Sokolov, M. M. Apodaca, B. A. Grzybowski, and I. S. Aranson, Proc. Natl. Acad. Sci. USA **107**, 969 (2010).
[21] E. M. Purcell, Am. J. Phys. **45**, 3 (1977).
[22] J. Happel and H. Brenner, *Low Reynolds Number Hydrodynamics* (Prentice Hall, Englewood Cliffs, 1965).
[23] A. Shapere and F. Wilczek, J. Fluid Mech. **198**, 557 (1989).
[24] M. E. J. Holwill, Phys. Aspects Flagellar Movement Physiological Rev. **46**, 696 (1966).
[25] T. L. Jahn and J. J. Votta, Annu. Rev. Fluid Mech. **4**, 93 (1972).
[26] J. Lighthill, *Mathematical Biofluiddynamics* (SIAM, Philadelphia, 1975).
[27] J. Lighthill, SIAM Rev. **18**, 161 (1976).
[28] J. J. Blum and M. Hines, Q. Rev. Biophys. **12**, 103 (1979).
[29] S. Childress, *Mechanics of Swimming and Flying* (Cambridge University Press, Cambridge, 1981).
[30] C. Brennen and H. Winet, Annu. Rev. Fluid Mech. **9**, 339 (1977).
[31] G. I. Taylor, Proc. R. Soc. London A **209**, 447 (1951).
[32] S. Ishijima, S. Oshio, and H. Mohri, Gamete Res. **13**, 185 (1986).
[33] I. R. Gibbons, J. Cell Biol. **91**, 107s (1981).
[34] B. Alberts, A. Johnson, J. Lewis, M. Raff, K. Roberts, and P. Walter, *Molecular Biology of the Cell*, 5th ed. (Garland Science, New York, 2007).
[35] G. I. Taylor, Proc. R. Soc. London A **211**, 225 (1952).
[36] H. D. M. Moore and D. A. Taggart, Biol. Reprod. **52**, 947 (1995).
[37] F. Hayashi, Funct. Ecol. **12**, 347 (1998).
[38] H. Moore, K. Dvoráková, N. Jenkins, and W. Breed, Nature (London) **418**, 174 (2002).
[39] X. L. Wu and A. Libchaber, Phys. Rev. Lett. **84**, 3017 (2000).
[40] L. H. Cisneros, R. Cortez, C. Dombrowski, R. E. Goldstein, and J. O. Kessler, Exp. Fluids **43**, 737 (2007).
[41] A. Sokolov, I. S. Aranson, J. O. Kessler, and R. E. Goldstein, Phys. Rev. Lett. **98**, 158102 (2007).
[42] Q. Liao, G. Subramanian, M. P. DeLisa, D. L. Koch, and M. M. Wu, Phys. Fluids **19**, 061701 (2007).
[43] S. Gueron, K. Levit-Gurevich, N. Liron, and J. J. Blum, Proc. Natl. Acad. Sci. USA **94**, 6001 (1997).
[44] M. Kim and T. R. Powers, Phys. Rev. E **69**, 061910 (2004).
[45] P. Lenz and A. Ryskin, Phys. Biol. **3**, 285 (2006).
[46] A. Vilfan and F. Jülicher, Phys. Rev. Lett. **96**, 058102 (2006).
[47] T. Ishikawa, M. P. Simmonds, and T. J. Pedley, J. Fluid Mech. **568**, 119 (2006).
[48] C. M. Pooley, G. P. Alexander, and J. M. Yeomans, Phys. Rev. Lett. **99**, 228103 (2007).
[49] V. B. Putz and J. M. Yeomans, J. Stat. Phys. **137**, 13 (2009).
[50] T. Niedermayer, B. Eckhardt, and P. Lenz, Chaos **18**, 037128 (2008).
[51] D. M. Woolley, R. F. Crockett, W. D. I. Groom, and S. G. Revell, J. Exp. Biol. **212**, 2215 (2009).

[52] L. J. Fauci, J. Comput. Phys. **86**, 294 (1990).
[53] Y. Yang, J. Elgeti, and G. Gompper, Phys. Rev. E **78**, 061903 (2008).
[54] G. J. Elfring and E. Lauga, Phys. Rev. Lett. **103**, 088101 (2009).
[55] G. J. Elfring and E. Lauga, Phys. Fluids **23**, 011902 (2011).
[56] G. J. Elfring and E. Lauga, J. Fluid Mech. **674**, 163 (2011).
[57] P. Moon and D. Spencer, *Field Theory for Engineers* (Van Nostrand Reinhold, New York, 1961).
[58] K. Sangtae, Int. J. Multiphase Flow **11**, 699 (1985).
[59] N. N. Lebedev, *Special Functions and Their Applications* (Dover Publisher, Englewood Cliffs, 1972).
[60] K. Sangtae and J. K. Seppo, *Microhydrodynamics, Principles and Selected Applications* (Dover Publication, New York, 2005).
[61] M. Sauzade, G. J. Elfring, and E. Lauga, Physica D **240**, 1567 (2011).
[62] S. Camalet, F. Julicher, and J. Prost, Phys. Rev. Lett. **82**, 1590 (1999).
[63] S. Camalet and F. Julicher, New J. Phys. **2**, 1 (2000).